Published in final edited form as:

ACS Appl Mater Interfaces. 2021 June 23; 13(24): 28764–28773. doi:10.1021/acsami.1c04895.

Antimicrobial Peptide-Loaded Pectolite Nanorods for Enhancing Wound-healing and Biocidal Activity of Titanium

Lan Zhang[1,2,†], **Yang Xue**[1,†], **Sanjana Gopalakrishnan**[2], **Kai Li**[1], **Yong Han**[1,*], **Vincent M. Rotello**[2,*]

[1]State-key Laboratory for Mechanical Behavior of Materials, Xi'an Jiaotong University, Xi'an 710049, China

[2]Department of Chemistry, University of Massachusetts Amherst, MA, 01003, USA

Abstract

Titanium is widely utilized for manufacturing medical implants due to its inherent mechanical strength and biocompatibility. Recent studies have focused on developing coatings to impart unique properties to Ti implants, such as antimicrobial behavior, enhanced cell adhesion and osteointegration. Ca and Si-based ceramic (CS) coatings can enhance bone integration through release of Ca and Si ions. However, high degradation rates of CS ceramics create a basic environment that reduces cell viability. Polymeric or protein-based coatings may be employed to modulate CS degradation. However, it is challenging to ensure coating stability over extended periods of time without compromising biocompatibility. In this study, we employed a fluorous-cured collagen shell as a drug-loadable scaffold around CS nanorod coatings on Ti implants. Fluorous-cured collagen coatings have enhanced mechanical and enzymatic stability and are able to regulate the release of Ca and Si ions. Furthermore, the collagen scaffold was loaded with antimicrobial peptides to impart antimicrobial activity while promoting cell adhesion. These multifunctional collagen coatings simultaneously regulate the degradation of CS ceramics and enhance antimicrobial activity, while maintaining biocompatibility.

Graphical Abstract

[*]**Corresponding Author:** Prof. Vincent M. Rotello, Department of Chemistry, University of Massachusetts, Amherst, MA, 01003, USA. rotello@chem.umass.edu, Prof. Yong Han, State-key Laboratory for Mechanical Behavior of Materials, Xi'an Jiaotong University, Xi'an 710049, China, yonghan@mail.xjtu.edu.cn.

Author Contributions

The manuscript was written through contributions of all authors. All authors have given approval to the final version of the manuscript.

[†]These authors contributed equally.

Supporting Information

The Supporting Information is available free of charge on the ACS Publications website. One PDF file contains – elemental composition analysis of all samples, Fluorescent imaging of cells adhered to all surfaces and live/dead assay, ECM mineralization study to estimate bone regeneration of each coating, and genetic sequencing.

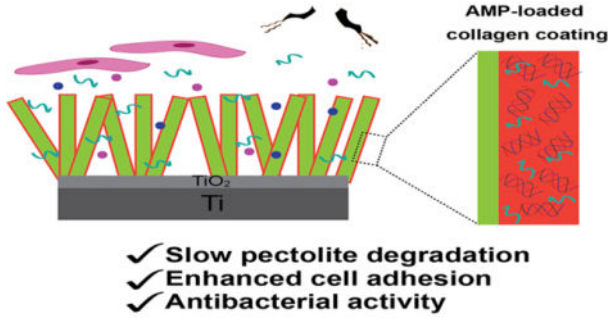

Keywords

$NaCa_2HSi_3O_9$ nanorods; pectolite coatings; collagen I; antimicrobial peptide; drug eluting coatings; cytocompatibility

INTRODUCTION

Titanium is widely utilized for manufacturing medical implants owing to its mechanical properties and biocompatibility. However, Ti is bio-inert and cannot resist bacterial invasion. Weak bone integration and bacterial infection are the two main causes of implant failure in clinic. Therefore, coating strategies are employed to impart properties such as anti-fouling behavior, enhanced osteointegration, and drug-loading to enhance wound-healing and prevent bacterial infections. For instance, Ca and Si based ceramic (CS) coatings have been developed to enhance bone integration through the release of Ca and Si ions during the degradation process.[1, 2, 3, 4, 5, 6, 7] Extracellular Ca^{2+} supply increases intracellular calcium level through Ca^{2+} channels, resulting in enhanced osteogenesis differentiation of osteoblasts.[2, 3] Si binds to glycosaminoglycan thereby crosslinking collagen and proteoglycan and acts as an initiator of osteoblast mineralization.[8, 9, 10] CS ceramics are also utilized as drug loadable scaffolds for delivering antimicrobial agents.[11] Unfortunately, high degradation rates of CS ceramics often cause increased basicity and low cell vitality.[12] Doping ions in the lattice (e.g. Zn, Sr and Cu) and compositing non-degradable components into CS ceramics are the two main strategies utilized to regulate degradation.[13, 14] However, ion doping amounts generally have threshold values due to their dose-dependent cytotoxicity. Incorporating components can increase the stability of CS-based matrix efficiently. The incorporated components include poly (lactic-co-glycolic acid), graphene oxide, TiO_2 and alginate etc. However, some of the incorporated components may be cytotoxic and therefore compromise biocompatibility.[4, 9, 12, 15, 16, 17]

Coatings on the CS ceramic layer may be employed to regulate degradation rate and impart multifunctionality to the implant.[7] Several protein-based coatings provide functionality such as antimicrobial behavior, wear-resistance, drug loadability, hydrophilicity and hydrophobicity.[18, 19, 20] Proteins are naturally occurring, biodegradable and biocompatible precursors which make them attractive for biomaterial coatings. However, they lack aqueous stability, exhibit poor mechanical strength, and rapidly degrade in enzymes. Collagen I (Col-I) is the major component of extracellular matrix in mammalian tissue, and has been widely used in biological modification of implants to enhance tissue repair.[18] Col-I is

biodegradable, biocompatible and can act as a drug-loadable scaffold,[19] but Col-I based matrixes or coatings directly formed by commercial Col-I solution are unstable in aqueous environments and lack sufficient mechanical strength and stability against proteolytic damage.[21]

Recently, we developed a thermal treatment strategy for stabilizing collagen films through the thermal curing of collagen films in a fluorous solvent-perfluoroperhydrophenanthrene (PFHP).[22] PFHP-based fluorous curing retains most of the protein secondary structure as compared to heat-cured films by minimizing rearrangement of proteins at the interface.[20, 22, 23] Consequently, fluorous-cured collagen films show enhanced mechanical and enzymatic stability while retaining protein structure and biocompatibility.[22] In this study, we utilized collagen-based films on a CS nanorod layer as multifunctional coatings for Ti implants. We hypothesized that fluorous-cured collagen coatings may act as a barrier to regulate the release of Ca and Si ions through the CS ceramic layer, while simultaneously enhancing cell adhesion. Furthermore, the collagen coating can act as a loadable scaffold for the release of antimicrobial agents including peptides.

Antimicrobial peptides (AMPs) exhibit potent and broad-spectrum antimicrobial activity, low cytotoxicity, and low immunogenicity.[24] AMPs have been successfully loaded in commercial collagen scaffolds and have demonstrated biocidal activity.[25] In this study, we developed multifunctional coatings for Ti implants by combining a pectolite nanorod coating and an AMP-loaded collagen shell. The PFHP-cured collagen shell is expected to regulate nanorod degradation thereby enhancing osteointegration while minimizing cytotoxicity. Incorporation and controlled release of AMPs imparts antimicrobial activity to the system. As shown in Figure 1, we fabricated pectolite nanorods (NCS) on Ti implants through micro arc oxidation (MAO) and hydrothermal treatment (HT). Following fabrication, collagen solutions containing AMPs were spin-coated and cured in PFHP to create a barrier for the ceramic surface as well as an antimicrobial coating. We demonstrated that PFHP treated collagen shells reduce degradation of nanorods and improve osteoblast behavior; the loaded AMP retains antibacterial activity after PFHP treatment and has long-lasting antibacterial activity.

RESULTS AND DISCUSSION

Microstructure of coatings

Ti substrates were first coated with pectolite nanorods by the protocol described in ref (6, 7). NCS consists of calcium sodium hydrogen silicate ($NaCa_2HSi_3O_9$, pectolite) and rutile. Cadoped TiO_2 was coated on Ti substrate by micro arc oxidation and then hydrothermally treated (HT) in an alkaline solution containing SiO_3^{2-} and Na^+. This alkaline environment causes migration of Ca^{2+} in TiO_2 to the coating surface and subsequent reaction with Na^+, SiO_3^{2-} and OH^- in the HT solution, forming pectolite nuclei. Prolonged HT treatment enabled growth of nuclei into nanorods. All the surfaces were covered by nanorods with an average diameter of 200 nm. They consisted of C, O, Ti, Ca, Si, Na and P (Table S1 and Figure 2). The amount of C detected on NCS was about 0.1At% (Figure 2), which is presumably due to adsorbed contamination. After spin-coating with pure Col-I (NCS-C) and Col-I incorporated with AMP (NCS-CA), the amounts of C increased to 1.8 and 3.7 %

respectively. PFHP treatment did not change the C amounts (NCS-C-P and NCS-CA-P are samples of NCS-C and NCS-CA after PFHP treatment respectively). Nanorod topography did not change in nano and micro scales (Figures 2 and S1 respectively) but thin webbed films could be observed between the nanorods (marked with arrows in Figure 2), indicating that Col-I formed conformal coatings on the nanorods. Treatment on NCS including spin-coating and fluorous-curing showed no significant change in its composition (linear graph in Figure 2).

Elemental compositions of coatings were verified using XPS, as shown in Figure 3. The bare NCS surfaces consisted of C, O, Ti, Si, P, Ca, and Na wherein C was ascribed to physical adsorption from the environment, Ti and P was from the dissolution of TiO_2 during formation of nanorods,6 and the other elements are attributed to the nanorods (Figure 3(a)). After spin-coating, peaks of Ti, Si, P, Ca, and Na decreased in strength, indicating the nanorods were covered. On the contrary, the peak strength of C increased significantly, and N was additionally detected, indicating presence of collagen. PHFP induced no obvious changes of C and N in peak strength and no new F peaks (600–700 eV) were observed. This confirms that PFHP is not incorporated into collagen film during treatment, consistent with our previous research.[22]

Analysis of XPS spectra further validated chemical compositions (Figure 3(b)). The high-resolution spectrum of C1s from different surfaces were deconvoluted into six peaks (Figure 3(c)), and they were centered at 283.3, 284.8, 286.1, 287.5, 288.3 and 289.3 eV corresponding to different chemical bonds. The main peak at 284.8 was ascribed to carbon-carbon backbones. The peaks at higher binding energies (e.g., 287.5, 288.3 and 289.3 eV) are typical of amide groups of carbon in collagen (C-O/O-C=O, N-C=O/C=O, C-C).[26, 27] The amounts of C and N detected by XPS and deconvoluted amide groups confirmed that nanorods had been successfully covered with Col-I as well as AMP.

The surface of NCS-CA-P was scratched to and observed on TEM to further evaluate the microstructure. The nanorods from NCS-CA-P (Figure 4(a)) are 200–300 nm in diameter, which are in accordance with those observed in Figure 2. The distinct spots in SAED pattern (Figure 4(b)) and inter-planar spacings of lattice fringes by HRTEM (Figure 4(c)) confirm that the nanorods are calcium sodium hydrogen silicate (NaCa2HSi3O9, pectolite, JCPDS card # 33-1223), indicating the PFHP treatment did not change the phase composition of nanorods. When the edges of nanorods were enlarged, a thin layer about 10 nm covering the nanorod was be observed on NCS-CA-P (Figure 4(d)). The squares marked with 1 and 2 in Figure 4(d) were detected by EDX, respectively (Figure S2). C amount in square 2 was much higher than that in square 1 (Figures 4(d) and S2), indicating that the thin layer was Col-I with AMP. Cu peaks were ascribed to the grid background.

Wettability and ion release

Surface hydrophilicity plays an important role in metal corrosion, protein adsorption as well as cell response.[7, 28] Hydrophobic coatings act as a barrier to protect the surface from corrosion.[28] The contact angles of different surfaces were measured as shown in Figure 5(a). The average contact angle is 63° on bare Ti. Pectolite nanorods greatly improve surface hydrophilicity due to the chemical composition and nanotopography.[29, 30] However, Col-I

coating increases the water contact angle to 60°. When Col-I was incorporated with AMP, NCS-CA has a much higher contact angle ~91°. After treatment in PFHP, the contact angles increase further as compared to the untreated ones which may be attributed to reorganization of collagen fibers, as explained in our previous work.[22]

The effect of the collagen shell on the degradation rate of the nanorods were evaluated by monitoring the ion release profile of NCS, NCS-C and NCS-C-P during prolonged immersion, as shown in Figures 5(b)–5(c). Initially, the concentrations of released Ca and Si follow the order: NCS>NCS-C>NCS-C-P. The concentration increased as immersion duration increased. The microstructures of nanorods on the three samples after immersion for 28 days were observed by SEM in Figures 5(d)–(f). Compared with those before immersion, nanorods were much sharper and thinner on NCS (Figure 5(d)), only slightly thinner on NCS-C (Figure 5(e)) and well-maintained on NCS-C-P (Figures 5(f)). Residual C can be detected on NCS-C and NCS-C-P. This residual C demonstrates that the Col-I layer after PFHP treatment can protect $NaCa_2HSi_3O_9$ nanorods from serious degradation during immersion. Previous research shows that as-prepared Col-I films are not water-stable.[21, 22] After treatment in PFHP, Col-I has a higher contact angle, and is more compact and stable than untreated collagen films and acts as a barrier in reducing the degradation reaction of $NaCa_2HSi_3O_9$ with H_2O.[31] Incorporation of AMP in the collagen shell should not significantly affect rate of degradation.[32] Previous research indicates that significant new bone formation on Ti implants is observed after ~ 4 weeks.[33] We therefore concluded that the collagen shell can successfully regulate NCS degradation for effective osteointegration after implantation.

AMP releasing and antibacterial property

Implant infections account for 45% of all nosocomial infections, often leading to implant failure, chronic infections, and tissue necrosis.[34] For this reason, multifunctional coatings that impart antibacterial activity while simultaneously enhancing osteointegration are being increasingly studied for medical implants. Previous research has demonstrated antibacterial activity through photodynamic/ sonodynamic therapy[35, 36, 37] or controlled release of ions (e.g., Ag^+ and Zn^{2+}) incorporated into implant coatings.[38, 39] However, photo-related or sonodynamic therapies need a sensitizer and excitation source to generate reactive oxygen species, and metal ions generally have dose-dependent antibacterial activity and cytotoxicity. We utilized AMPs owing to their broad-spectrum activity, low cytotoxicity, and immunogenicity and loadability into collagen scaffolds.[24, 25]

Ideally, a localized drug should exhibit a high concentration burst release for effective protection against infection and prevention of drug-resistance, followed by a prolonged release for effective eradication of bacteria.[40, 41] The release of AMP by NCS-CA and NCS-CA-P were evaluated and shown in Figure 6(a). Burst release as well as prolonged release of AMPs was observed from both samples. More AMP was released from NCS-CA than from NCS-CA-P. AMP release was mainly controlled by molecular diffusion and the degradation of the coating.[27] PFHP treatment made Col-I more stable which resulted in the sustained release of AMP from NCS-CA-P, compared to NCS-CA.

As PFHP treatment was conducted at 180 °C, the stability of the AMPs to the treatment conditions was evaluated through measuring antibacterial efficacy against planktonic and adherent *S. aureus* for NCS-CA-P and NCS-CA before and after immersion in 0.9 wt% NaCl (PBS) solution for 28 days (Figure 6(b)). Bare Ti has no antibacterial activity and was used as control. As prepared NCS-CA-P and NCS-CA exhibit good antibacterial activity against both planktonic and adherent *S. aureus*. Contact-killing activity (Ra) and antibacterial-release activity (Rp) for the two sample are almost 100%. After immersion, as part of AMP was released from the surface, antibacterial activity of NCS-CA and NCS-CA-P both decreased (**Marked in red sample labels in** Figure 6(b)). About 60% of adherent bacteria and 50% planktonic bacteria were also killed by NCS-CA-P, which was much higher than NCS-CA. *S. aureus* adhesion on coated and uncoated surfaces after 24 h of culture were further confirmed by live/dead assay and SEM imaging, as shown in Figure 6(c). *S. aureus* with smooth and intact surfaces were observed on Ti (stained green). However, mostly dead bacteria (stained red) were observed on as prepared NCS-CA and NCS-CA-P. After immersion, more live bacteria were seen on NCS-CA than on NCS-CA-P, which can be attributed to quicker release of AMP from NCS-CA as compared to NCS-CA-P (Figure 6(a)). AMP penetrates bacterial membrane, leading to the leakage of intracellular substance and eventual death of bacteria.[24] Damaged bacterial membranes were observed on the AMP loaded samples through SEM and further confirmed the antibacterial activity from AMP release (**marked with arrows in** Figure 6(c)). We therefore concluded that AMP maintained activity post PFHP treatment at 180 °C and endow the collagen shell with long-lasting biocidal activity.

In vitro osteoblast response evaluation

Cell viability was evaluated through the MTT assay which measures the mitochondrial activity of hFOB1.19 on different surfaces after incubation for 1, 3 and 6 days, as shown in Figure 7(a). After 1 d of incubation, cells growing on nanorods with a Col-I shell (NCS-C and NCS-C-P) showed higher mitochondrial activity than those on bare nanorods-coated Ti (NCS). When Col-I was incorporated with AMP, mitochondrial activity of cells was reduced on NCS-CA, but no obvious change was observed on NCS-CA-P. Osteoblast viability is significantly enhanced when pH value is around 8–8.5,[42] but higher pH can be harmful to cells and diminish viability.[43] Collagen shell reduces the degradation of NCS nanorods thereby increasing cell adhesion. While increasing the concentration of AMP improves antibacterial activity, it compromises the cytocompatibility.

The dosage and release rate of AMPs must be controlled. The burst release of AMP from the unstable Col-I (NCS-CA) inhibited cell adhesion. After 3 d of incubation, the mitochondrial activity of cells was highest on Ti, followed by the PFHP treated, the PFHP untreated and bare nanorods. After 6 d of incubation mitochondrial activity of cells on NCS was much lower than that on Ti, indicating poor cytocompatibility. PFHP treated samples had similar mitochondrial activity of cells with Ti and higher than those on the PFHP untreated (NCS-C and NCS-CA).

The distributions and viabilities of cells seeded on different surfaces after 1 and 3 days of incubation were further confirmed by live/dead staining. The dead cells were counted in

Figure 7(b) and Figure S3 shows the distribution of dead cells after 1 d of incubation on different surfaces by a microscope. The dead cells were observed on NCS whether at 1 d and 3 d of incubation. Col-I coatings, especially after PFHP treatment, showed more live cells as compared to bare nanorods. The morphologies of cells after 1 day of culture were observed through actin-nucleus staining fluorescence (Figure 8) and SEM (Figure S5). Most cells on Ti were elongated, indicating that they did not spread well on the surface. The cells adhering on NCS-C, NCS-C-P and NCS-CA-P displayed typically polygonal morphologies and organized filamentous actin bundles, indicating that they spread well. On NCS or NCS-CA, although the cells were polygonal, the filamentous actin bundles were thinner and fewer in number indicating poor adhesion (**left two rows in** Figure 8).

Combining the degradation behavior and cell cytocompatibility assessment (Figures 6(a), 7 and 8), we concluded that bare nanorods could not support osteoblast growth. Collagen shell contributed to increased cytocompatibility on nanorods. When AMP, burst release of AMP was incorporated in the shell, cytocompatibility decreased due to AMP cytotoxicity (NCS-CA) however, PFHP treatment is able to mitigate this by effectively regulating AMP release.Based on the results in Figures 7 and 8, NCS-C-P and NCS-CA-P were selected to evaluate the osteogenesis function of osteoblasts. Expressions of osteogenesis-related genes in the cells on NCS-C-P and NCS-CA-P were monitored for 14 days, as shown Figure 9 (Ti was used as a control). It is known that Runx2 is a transcription factor for early differentiation of osteoblast. ALP, OPN, and OCN are the early, middle, and late-stage markers of osteoblast differentiation. Their expression indicated that NCS-C-P and NCS-CA-P accelerated the cell differentiation compared with uncoated Ti. Stabilized collagen shell protects the pectolite nanorods from rapid degradation (Figure 5) in addition to reduced burst release of AMP (Figure 6(a)). The sustained release of Ca and Si combined with the surface nanotopography contribute to improved osteoblast differentiation (Figure 9) and ECM mineralization (Figure S4) on NCS-CA-P and NCS-C-P.

CONCLUSION

Pectolite nanorods effectively release Ca and Si ions but hamper cell adhesion and growth due to acute cytotoxicity from rapid degradation. Fluorous-cured collagen coatings allowed regulation of the rate of nanorod degradation, thereby controlling Ca and Si ions in the environment. Collagen coating also enhances cytocompatibility of the implant. Furthermore, Col-I coating acts as a loadable scaffold for antimicrobial peptides that impart antibacterial activity to the implant and act as a barrier to reduce degradation of nanorods. Pectolite nanorods with AMP-doped Col-I shell have both osteoblast response and antimicrobial activity. Overall, this study demonstrates a novel strategy for fabrication of highly effective multifunctional coatings for bone regeneration applications using a pectolite nanorod coating with a collagen shell.

EXPERIMENTAL METHODS

Preparation of the CS nanorod (NCS) coating

Commercially obtained pure Ti (Ø 14×2 mm, 99.99 wt%) was micro arc oxidized (MAO) as an anode for 3 min by a pulsed power supply with an applied voltage of 500 V, a pulse

frequency of 500 Hz, and a duty ratio of 7.5%. The electrolyte contains 0.3 M calcium acetate, 0.03 M β glycerophosphate disodium and 1.25% acetic acid. After MAO treatment, the samples were immediately washed with distilled water and hydrothermally treated in an aqueous solution containing 2M Na2SiO3 and NaOH at 240 °C for 24 h. The obtained samples were ultrasonically washed in distilled water, dried in air, and labelled NCS (Ca-Si nanorod coating).

Structural characterization of the coatings

Surface morphologies and element composition were measured by a field emission scanning electron microscope (FESEM, JSM-6700F, JEOL, Japan) equipped with an energy dispersive X-ray spectrometer (EDX; DX-4, Philips, Netherlands). Phase components were analyzed by X-ray diffraction (X'Pert PRO, PANalytical Co., The Netherlands) using Cu Kα rays. Chemical species of different surfaces were evaluated by a monochromatic X-ray photoelectron spectroscope (XPS; Axis Ultra, UK) with Mg-Kα radiation as an X-ray source and the photoelectron take-off angle was set at 45°. C1s (hydrocarbon C/C, C/H, 284.8 eV) was used to a standard.

Evaluation of wettability, ion, and AMP release from the coatings

The wettability of coatings was measured using a surface contact angle measurement technique (DSA30, Kruss, Germany). A single drop of distilled water distilled water (2.5 μL) was dropped onto each sample and high-resolution images were obtained. Captured images were utilized to estimate the contact angles through the analysis software (DSAI).

For measuring the release of Ca and Si ions, NCS, NCS-C and NCS-C-P were separately immersed in 1 mL 0.9 wt% NaCl (PS) solution at 37 °C for 1–28 days, successively. At the pre-determined time points, the supernatant was collected, and the solution was replaced. The refreshment of the supernatant at the pre-determined timepoints is crucial to maintain the pH of the coating environment. As the nanorods degrade, the pH of the solution increases which may affect the rate of degradation of the nanorods. Furthermore, refreshment of supernatant is closer to the *in vivo* environment where constant flow of biological fluids is expected to regulate the pH of the environment. The concentrations of Ca and Si ions released were measured by inductively coupled plasma-mass spectrometry (ICP-MS; Nu Instruments, Wrexham, UK).

For the AMP release study, different concentrations of HHC-36 was dissolved in PS to prepare a series of standard solutions. A calibration curve was obtained by fitting the measured absorbance values at 279 nm (Thermo Scientific Multiskan GO) versus the corresponding AMP concentrations. NCS-CA and NCS-CA-P were immersed 1 mL of PS for 0–28 days at 37 °C. At each pre-determined time, the absorbance of resultant solution was measured at wavelength of 279 nm, and the AMP concentrations were calculated based on the calibration curve.

In vitro cytocompatibility of osteoblast

Osteoblasts (hFOB1.19) purchased from the Institute of Biochemistry and Cell Biology of Chinese Academy of Sciences (Shanghai, China) were inoculated in Dulbecco's modified

Eagle's medium (DMEM; HyClone, USA) supplemented with 10% fetal bovine serum (HyClone, USA), 1.2 mg/mL Na_2CO_3, 0.5 mM sodium-pyruvate (Sigma, USA), and 0.3 mg/mL Geneticine418 (Sigma, USA) in a humidified atmosphere incubator with 5% CO_2 at 37 °C. The Medium was refreshed every 2 days.

hFOB1.19 cells were seeded on each sample at a density of 2×10^4 cells/well and incubated for 1, 3 and 6 days, according to the instruction which has been described elsewhere.[7] Each test was repeated four times. Live/dead viability/cytotoxicity kit (Invitrogen, Eugene, OR) was used to identify viable and dead cells on different samples after 1 and 3 days of culture. Epifluorescence images were obtained on an Olympus BX52 microscope. The cell morphologies on different sample after incubation for 1 d were also observed. The cell-adhered samples were washed with PBS for three timed, fixed with 2.5% glutaraldehyde at 4 °C, dehydrated in ethanol, dried in vacuum, coated with gold, and observed by FESEM.

Actins and cell nucleus were stained with a staining kit (FAK100, Millipore, USA) after 24 h of incubation on different surfaces. Cells were fixed with 4% paraformaldehyde, and permeabilized by 0.1% Triton X-100 (Sigma, USA). Then 37.5 ng/mL TRITC-conjugated phalloidin were added and were incubated at 37 °C for 60 min for actin staining. After washed three times using PBS buffer, that, 0.1 ng/mL 6-diamidino-2-phenylindole (DAPI) was added in each well and incubated in at 37 °C for 5 min to stain cell nucleus. Finally, the samples were washed three times using PBS buffer and observed by an epifluorescence (SMZ745T, Nikon, Japan).

TRIzol reagent ((Life Technologies, USA) was used to isolate total RNA from each sample after 14 days of incubation. The obtained RNA was reverse transcribed into complementary DNA using a PrimeScript RT reagent kit (Abcam, UK). The expression of osteogenic differentiation markers such as Alkaline phosphatase (ALP), runt-related transcription factor 2 (Runx2), osteopontin (OPN), osteocalcin (OCN) and collagen I (Col-I) were quantified by LightCycler 96 real-time PCR instrument (Roche, Switzerland) with SYBR FastStart Essential DNA Green Master Mix (Roche, Switzerland). The housekeeping gene glyceraldehyde-3-phosphate dehydrogenase (GAPDH) was used as endogenous reference to normalize calculation through the $2^{-\Delta\Delta CT}$ method. The sequences of specific primer sets was shown in Table S2.

In vitro antibacterial test

Staphylococcus aureus (S. aureus, ATCC 25293) were inoculated to obtain bacteria in the midlogarithmic phase of growth, and then suspended in Mueller Hinton Broth to a final concentration of ~1×105 colony-forming units/ mL.

The AMP-loaded samples (NCS-CA and NCS-CA-P) and those after 28 days of immersion in PBS were employed to evaluate the short- and long-term antibacterial activity, respectively. Bare Ti was evaluated as control. 1 mL of bacterial solution was added in each well with a sample. After incubation at 37 °C for 24 h, the planktonic survivals in the resultant solutions were measured according to the National Standard of China GB/T 4789.2 protocol to evaluate the antibacterial activity due to AMP release. Simultaneously, the samples were rinsed three times by PBS and the adhered bacteria were detached

by ultrasonic vibration in 1 mL of PBS for 5 min. The obtained bacterial solutions were sampled to measure the viable bacteria to evaluate the contact-killing activity. The AMP release-based antimicrobial activity of different coatings were calculated as Rp (%) = (B−A)/B×100%, where A and B are the number of viable bacteria in the solutions incubated with the samples and control, respectively, whereas the contact-killing behavior was calculated as Ra (%) =(D−C)/D×100%, where C and D are the number of viable bacteria on the coating and Ti, respectively.

A Live/Dead Backlight Bacterial Viability Kit (L13152) was used for quantifying adherent cell viability on each substrate after 24 h of culture according to the instruction. Fluorescent images were obtained by an Olympus BX52 microscope. Bacterial morphologies on the samples after cultured for 24 h were also observed by SEM following the same instruction of cell described in Section 2.4.

Statistical analysis

SPSS 14.0 software (SPSS, USA) was used to analyze the data. The level of significance was determined by a one-way ANOVA followed with a Student-Newman-Keuls post hoc test. $p<0.05$ and $p<0.01$ were considered to be significant and highly significant, separately. Data are presented as the mean ± SD, n=4.

Supplementary Material

Refer to Web version on PubMed Central for supplementary material.

Funding Sources

LZ, YX and KL greatly appreciate the support of the National Natural Science Foundation of China (Grant number 51771142). LZ also acknowledges the support of National Key Research and Development Program of China No. 2016YFC1100600 (sub-project 2016YFC1100604) and Natural Science Basic Research Program of Shaanxi Province (No. 2020JM-024). YH acknowledges the financial support provided by the National Natural Science Foundation of China (Grant numbers 51971171 and 51631007). VMR and SG acknowledge support from the NIH (AI AI134770) for research performed at the University of Massachusetts.

ABBREVIATIONS

ALP	alkaline phosphatase
AMPs	Antimicrobial peptides
CS	Ca and Si-based ceramic
Col-I	Collagen I
DMEM	Dulbecco’s modified Eagle’s medium
HHC-36	KRWWKWRR-NH2
EDX	energy dispersive X-ray spectrometer
FESEM	field emission scanning electron microscope
HT	hydrothermal treatment

MAO	micro arc oxidation
NCS	pectolite nanorods
NCS-C	NCS spinning coated with collagen I
NCS-CA	NCS spinning coated with collagen I and AMP
NCS-C-P	NCS-C experienced PFHP treatment
NCS-CA-P	NCS-CA experienced PFHP treatment
OPN	osteopontin
OCN	osteocalcin
PS	0.9 wt% NaCl solution
PFHP	perfluoroperhydrophenanthrene
Ra	contact-killing activity
Rp	antibacterial-release activity
XPS	X-ray photoelectron spectroscope
Runx2	runt-related transcription factor 2

REFERENCES

(1). Rather HA; Jhala D; Vasita R Dual Functional Approaches for Osteogenesis Coupled Angiogenesis in Bone Tissue Engineering. Mater. Sci. Eng., C 2019, 103, 109761.

(2). Gao JY; Wang M; Shi C; Wang LP; Wang DL; Zhu YC Synthesis of Trace Element Si and Sr Co-doping Hydroxyapatite with Non-cytotoxicity and Enhanced Cell Proliferation and Differentiation. Biol. Trace Elem. Res 2016, 174, 208–217. [PubMed: 27075548]

(3). Cheng HY; Hu H; Li G; Zhang M; Xiang KW; Zhu ZH; Wan Y Calcium Titanate Micro-Sheets Scaffold for Improved Cell Viability and Osteogenesis. Chem. Eng. J 2020, 389, 124400.

(4). Xiong K; Wu TT; Fan QB; Chen L; Yan MH Novel Reduced Graphene Oxide/Zinc Silicate/Calcium Silicate Electroconductive Biocomposite for Stimulating Osteoporotic Bone Regeneration. ACS Appl. Mater. Interfaces 2017, 9 (51), 44356–44368. [PubMed: 29211449]

(5). Zhang J; Wang HM; Shi J; Wang Y; Lai KC; Yang XY; Chen XY; Yang GL Combination of Simvastatin, Calcium Silicate/Gypsum, and Gelatin and Bone Regeneration in Rabbit Calvarial Defects. Sci. Rep 2016, 6, 23422. [PubMed: 26996657]

(6). Zhang L; Huang XY; Han Y Formation Mechanism and Cytocompatibility of Nano-shaped Calcium Silicate Hydrate/Calcium Titanium Silicate/TiO_2 Composite Coatings on Titanium. J. Mater. Chem. B 2016, 4 (41), 6734–6745. [PubMed: 32263528]

(7). Li K; Xue Y; Zhou JH; Han J; Zhang L; Han Y Silanized $NaCa_2HSi_3O_9$ Nanorods with a Reduced pH Increase on Ti for Improving Osteogenesis and Angiogenesis *in vitro*. J. Mater. Chem. B 2020, 8 (4), 691–702. [PubMed: 31867581]

(8). Huang Y; Zhang HL; Qiao HX; Nian XF; Zhang XJ; Wang WD; Zhang XY; Chang XT; Han SG; Pang XF Anticorrosive Effects and *in vitro* Cytocompatibility of Calcium Silicate/Zinc-doped Hydroxyapatite Composite Coatings on Titanium. Appl. Surf. Sci, 357, 1776–1784.

(9). Qian GW; Lu TL; Zhang J; Liu R; Wang ZZ; Yu B; Li HY; Shi HS; Ye JD Promoting Bone Regeneration of Calcium Phosphate Cement by Addition of PLGA Microspheres and

Zinc Silicate via Synergistic Effect of *in-situ* Pore Generation, Bioactive Ion Stimulation and Macrophage Immunomodulation. Appl. Mater. Today 2020, 19, 100615.

(10). Xiong K; Zhang J; Shi HS; Liu JQ; Wu H; Li HY; Ye JD Preparation and *in vitro* Cell-biological Performance of Sodium Alginate/Nano-Zinc Silicate Co-modified Calcium Silicate Bioceramics. RSC Adv. 2015, 5 (11), 8329–8339.

(11). Kordjamshidi A; Saber-Samandari S; Ghadiri Nejad MG; Khandan A Preparation of Novel Porous Calcium Silicate Scaffold Loaded by Celecoxib Drug using Freeze Drying Technique: Fabrication, Characterization, and Simulation. Ceram. Int 2019, 45 (11), 14126–14135.

(12). Chiu CK; Lee DJ; Chen H; Chow LC; Ko CC *In-situ* Hybridization of Calcium Silicate and Hydroxyapatite-Gelatin Nanocomposites Enhances Physical Property and *in vitro* Osteogenesis. J. Mater. Sci.: Mater. Med 2015, 26, 92. [PubMed: 25649517]

(13). Li K; Hu DD; Xie YT; Huang LP; Zheng XB Sr-doped Nanowire Modification of Ca-Si-based Coatings for Improved Osteogenic Activities and Reduced Inflammatory Reactions. Nanotechnology 2018, 29 (8), 084001. [PubMed: 29256438]

(14). Ma R; Yu ZF; Tang SC; Pan YK; Wei J; Tang TT Osseointegration of Nanohydroxyapatite- or Nanocalcium Silicate-incorporated Polyetheretherketone Bioactive Composites *in vivo*. Int. J. Nanomed 2016, 11, 6023–6033.

(15). Heimann RB Plasma-Sprayed Hydroxylapatite-Based Coatings: Chemical, Mechanical, Microstructural, and Biomedical Properties. J. Therm. Spray. Tech 2016, 25 (5), 827–850.

(16). Zheng A; Cao LY; Liu Y; Wu JN; Zeng DL; Hu LW; Zhang XK; Jiang XQ Biocompatible Silk/Calcium silicate/Sodium Alginate Composite Scaffolds for Bone Tissue Engineering. Carbohyd. Polym 2018, 199, 244–255.

(17). Mehrali M; Akhiani AR; Talebian S; Mehrali M; Latibari ST; Dolatshahi-Pirouz A; Metselaar HSC Electrophoretic Deposition of Calcium Silicate–reduced Graphene Oxide Composites on Titanium Substrate. J. Eur. Ceram. Soc 2016, 36 (2), 319–332.

(18). Zhang DW; Wu XW; Chen JD; Lin KL The Development of Collagen-based Composite Scaffolds for Bone Regeneration. Bioact. Mater 2018, 3 (1), 129–138. [PubMed: 29744450]

(19). Dong X; Liu HJ; Feng HY; Yang SC; Liu XL; Lai X; Lu Q; Lovell JF; Chen HZ; Fang C Enhanced Drug Delivery by Nanoscale Integration of a Nitric Oxide Donor to Induce Tumor Collagen Depletion. Nano Lett. 2019, 19 (2), 997–1008. [PubMed: 30676760]

(20). Wang LS; Gopalakrishnan S; Lee YW; Zhu JX; Nonnenmann SS; Rotello VM Translation of Protein Charge and Hydrophilicity to Materials Surface Properties Using Thermal Treatment in Fluorous Media. Mater. Horiz 2018, 5 (2), 268–274

(21). Sun LL; Li BF; Yao D; Song WK; Hou H Effects of cross-linking on mechanical, biological properties and biodegradation behavior of Nile tilapia skin collagen sponge as a biomedical material. J. Mech. Behav. Biomed. Mater 2018, 80, 51–58. [PubMed: 29414475]

(22). Zhang L; Gopalakrishnan S; Li K; Wang LS; Han Y; Rotello VM Fabrication of Collagen Films with Enhanced Mechanical and Enzymatic Stability through Thermal Treatment in Fluorous Media. ACS Appl. Mater. Interfaces 2020, 12 (5), 6590–6597. [PubMed: 31935058]

(23). Gopalakrishnan S; Xu JL; Zhong F; Rotello VM Strategies for Fabricating Protein Films for Biomaterial Applications. Adv. Sustainable Syst 2021, 5, 2000167. [PubMed: 33709022]

(24). Kumar P; Kizhakkedathu JN; Straus SK Antimicrobial Peptides: Diversity, Mechanism of Action and Strategies to Improve the Activity and Biocompatibility *in vivo*. Biomolecules 2018, 8 (1), 4.

(25). Lozeau LD; Grosha J; Kole D; Prifti F; Dominko T; Camesano TA; Rolle MW Collagen Tethering of Synthetic Human Antimicrobial Peptides Cathelicidin LL37 and its Effects on Antimicrobial Activity and Cytotoxicity. Acta Biomater. 2017, 52, 9–20. [PubMed: 28017866]

(26). O'Neill L; Dobbyn P; Kulkarni M; Pandit A Wound Healing using Plasma Modified Collagen. Clinical Plasma Medicine 2018, 12, 23–32.

(27). Qiang TT; Chen L; Yan Z; Liu XH Evaluation of a Novel Collagenous Matrix Membrane Cross-Linked with Catechins Catalyzed by Laccase: A Sustainable Biomass. J. Agric. Food Chem 2019, 67 (5), 1504–1512. [PubMed: 30644748]

(28). Nakamura M; Hori N; Ando H; Namba S; Toyama T; Nishimiya N; Yamashita K Surface Free Energy Predominates in Cell Adhesion to Hydroxyapatite Through Wettability. Mat. Sci. Eng. C-Mater 2016, 62, 283–292.

(29). Khandan A; Abdellahi M; Ozada N; Ghayour H Study of the Bioactivity, Wettability, and Hardness Behaviour of the Bovine Hydroxyapatite-diopside Bio-nanocomposite Coating. J. Taiwan Inst. Chem. Eng 2016, 60, 538–546.

(30). Li J; Tan L; Liu XM; Cui ZD; Yang XJ; Yeung KWK; Chu PK; Wu SL Balancing Bacteria-Osteoblast Competition through Selective Physical Puncture and Biofunctionalization of ZnO/Polydopamine/Arginine-Glycine-Aspartic Acid-Cysteine Nanorods. ACS Nano. 2017, 11 (11), 11250–11263. [PubMed: 29049874]

(31). Liu WJ; Zhai D; Huan ZG; Wu CT; Chang J Novel Tricalcium Silicate/magnesium Phosphate Composite Bone Cement having High Compressive Strength, *in vitro* Bioactivity and Cytocompatibility. Acta Biomater. 2015, 21, 217–227. [PubMed: 25890099]

(32). Lin ZF; Wu TT; Wang WS; Li BL; Wang M; Chen LL; Xia H; Zhang T Biofunctions of Antimicrobial Peptide-Conjugated Alginate/Hyaluronic Acid/Collagen Wound Dressings Promote Wound Healing of a Mixed-bacteria-infected Wound. Int. J. Biol. Macromol 2019, 140, 330–342. [PubMed: 31421174]

(33). He Y; Mu CY; Shen XK; Yuan Z; Liu J; Chen WZ; Lin CC; Tao BL; Liu B; Cai KY Peptide LL-37 Coating on Micro-structured Titanium Implants to Facilitate Bone Formation *in vivo* via Mesenchymal Stem Cell Recruitment. Acta Biomater. 2018, 80, 412–424. [PubMed: 30266635]

(34). Schierholz JM; Beuth J Implant Infections: A Haven for Opportunistic Bacteria. J. Hosp. Infect 2001, 49, 87–93. [PubMed: 11567552]

(35). Su K; Tan L; Liu XM; Cui ZD; Zheng YF; Li B; Han Y; Li ZY; Zhu SL; Liang YQ; Feng XB; Wang XB; Wu SL Rapid Photo-Sonotherapy for Clinical Treatment of Bacterial Infected Bone Implants by Creating Oxygen Deficiency Using Sulfur Doping. ACS Nano 2020, 14 (2), 2077–2089. [PubMed: 31990179]

(36). Guan W; Tan L; Liu XM; Cui ZD; Zheng YF; Yeung KWK; Zheng D; Liang YQ; Li ZY; Zhu SL; Wang XB; Wu SL Ultrasonic Interfacial Engineering of Red Phosphorous-Metal for Eradicating MRSA Infection Effectively. Adv. Mater 2021, 33 (5), 2006047.

(37). Li M; Li LQ; Su K; Liu XM; Zhang TJ; Liang YQ; Jing DD; Yang XJ; Zheng D; Cui ZD; Li ZY; Zhu SL; Yeung KWK; Zheng YF; Wang XB; Wu SL Highly Effective and Noninvasive Near-Infrared Eradication of a Staphylococcus aureus Biofilm on Implants by a Photoresponsive Coating within 20 Min. Adv. Sci 2019, 6 (17), 1900599.

(38). Zhang YZ; Liu XM; Li ZY; Zhu SL; Yuan XB; Cui ZD; Yang XJ; Chu PK; Wu SL Nano Ag/ZnO Incorporated Hydroxyapatite Composite Coatings: Highly Effective Infection Prevention and Excellent Osteointegration. ACS Appl. Mater. Interfaces 2018, 10 (1),1266–1277. [PubMed: 29227620]

(39). Xie XZ; Mao CY; Liu XM; Tan L; Cui ZD; Yang XJ; Zhu SL; Li ZY;Yuan XB; Zheng YF; Yeung KWK; Chu PK; Wu SL Tuning the Bandgap of Photo-Sensitive Polydopamine/Ag_3PO_4/Graphene Oxide Coating for Rapid, Noninvasive Disinfection of Implants. ACS Cent. 2018, 4 (6), 724–738.

(40). Wang TT; Liu XM; Zhu YZ; Cui ZD; Yang XJ; Pan HB; Yeung KWK; Wu SL Metal Ion Coordination Polymer-Capped pH-Triggered Drug Release System on Titania Nanotubes for Enhancing Self-antibacterial Capability of Ti Implants. ACS Biomater. Sci. Eng 2017, 3 (5), 816–825. [PubMed: 33440485]

(41). Zhang YN; Zhang L; Li B; Han Y Enhancement in Sustained Release of Antimicrobial Peptide from Dual-Diameter-Structured TiO_2 Nanotubes for Long-Lasting Antibacterial Activity and Cytocompatibility. ACS Appl. Mater. Interfaces 2017, 9 (11), 9449–9461. [PubMed: 28240853]

(42). Li QW; Wang DH; Qiu JJ; Peng F; Liu XY Regulating the Local pH Level of Titanium via Mg-Fe Layered Double Hydroxides Films for Enhanced Osteogenesis. Biomater. Sci 2018, 6 (5), 1227–1237. [PubMed: 29589018]

(43). Li B; Han Y; Qi K Formation Mechanism, Degradation Behavior, and Cytocompatibility of a Nanorod-shaped HA and Pore-sealed MgO Bilayer Coating on Magnesium. ACS Appl. Mater. Interfaces 2014, 6 (20), 18258–18274. [PubMed: 25265530]

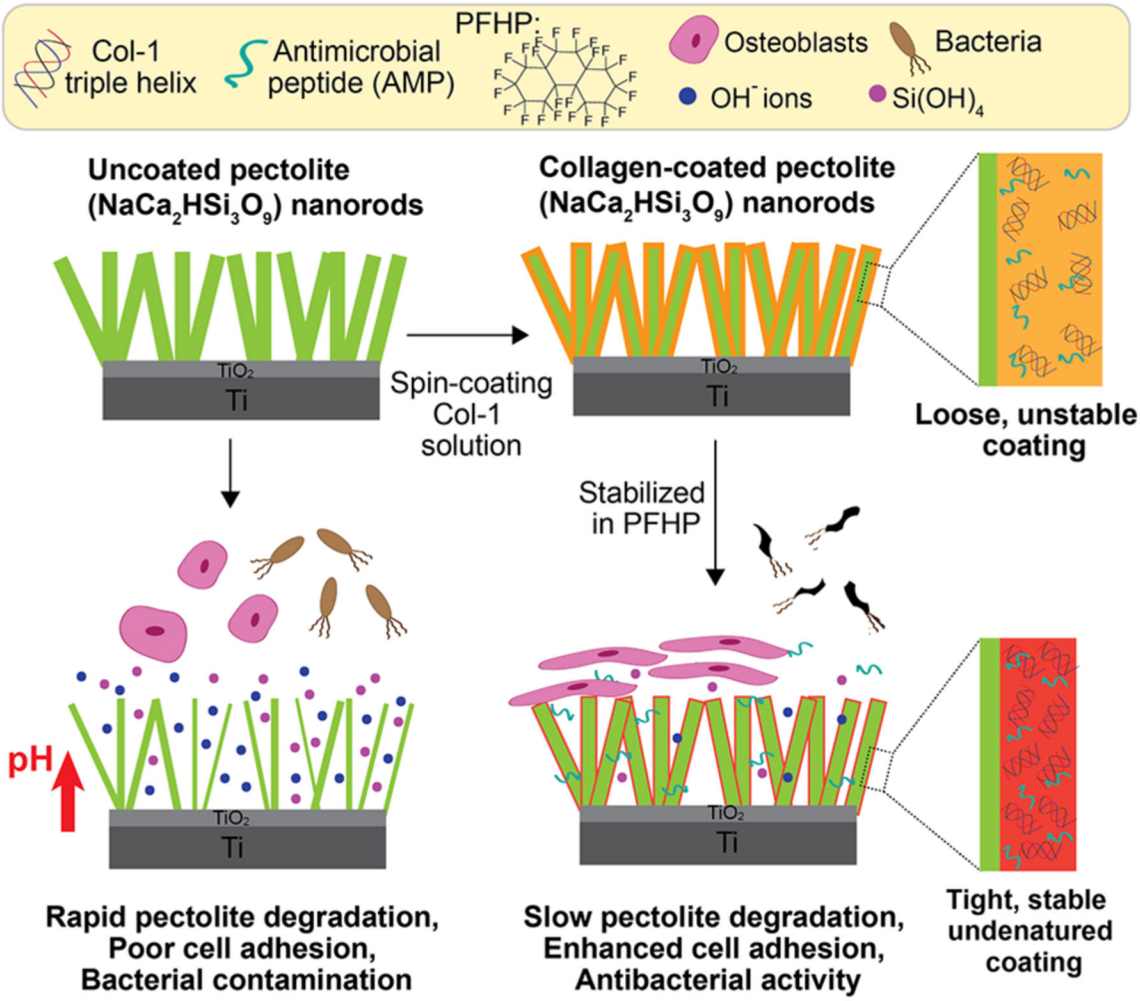

Figure 1.

Schematic depicting the fabrication of collagen coatings. Pectolite ($NaCa_2HSi_3O_9$) nanorods are first coated on Ti implant., then collagen I (Col-I) doped with antimicrobial peptide (AMP) is spin-coated onto the nanorods, and then heated in fluorous solvent (PFHP) for stabilization. The Col-I shell not only slows down the NCS degradation, but also acts as a scaffold for loading and controlled release of AMP.

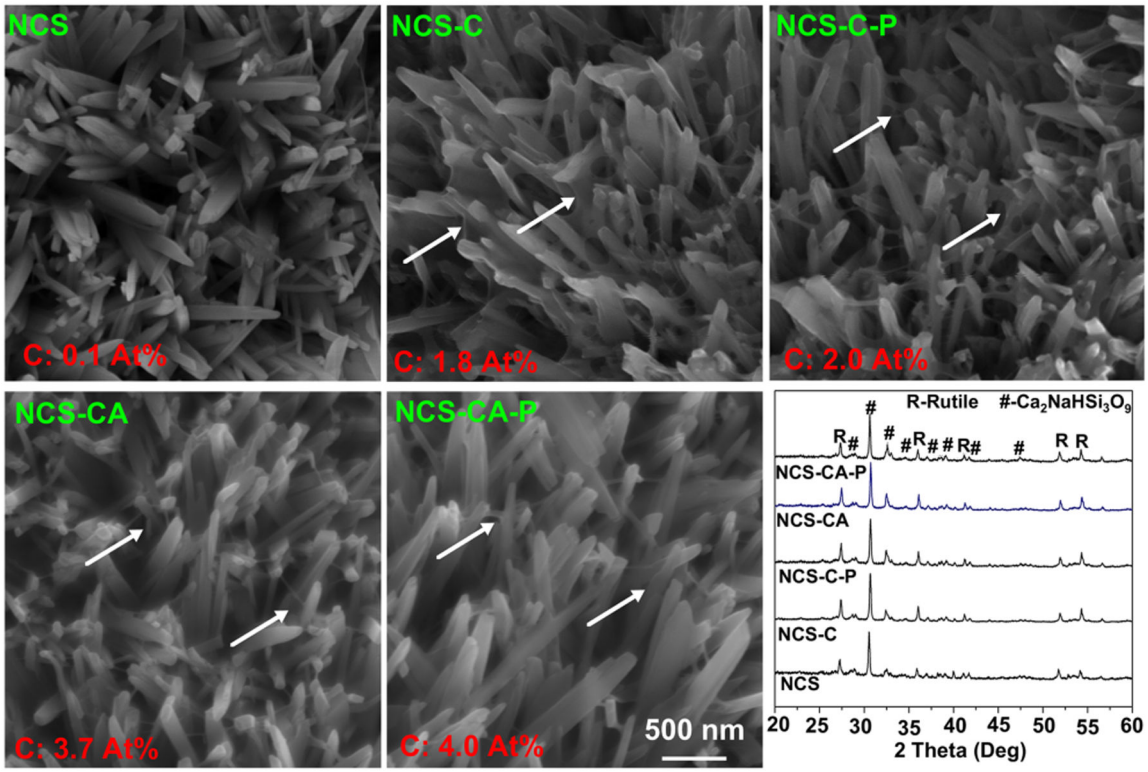

Figure 2.

Surface morphologies of nanorods (NCS), collagen-coated NCS with (NCS-CA) and without (NCS-C) AMP, and PFHP-cured collagen coatings (NCS-C-P and NCS-CA-P). Collagen coating results in weblike films between nanorods as depicted by white arrows in the SEM images. Average C content is seen in red in the images and in XRD patterns of different samples. As expected, C content increased with incorporation of Collagen and AMP on the surface.

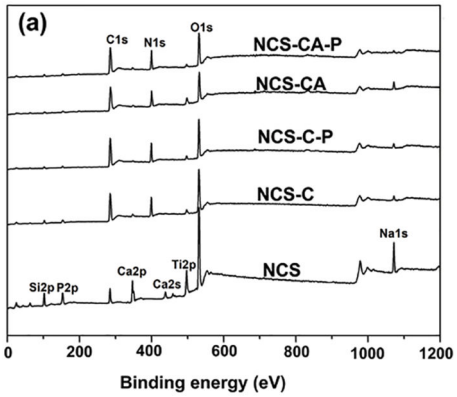

(b)

Elemental composition (At%)	Sample				
	NCS	NCS-C	NCS-C-P	NCS-CA	NCS-CA-P
O	47.02	24.39	20.80	19.33	19.91
C	18.44	51.91	55.99	53.74	55.35
N	/	14.99	15.89	15.58	15.85
Na	7.31	1.52	1.69	2.80	1.07
Si	19.13	5.78	3.17	2.99	3.58
Ca	6.90	1.10	0.98	0.78	0.88
P	0.6	/	/	/	/
Ti	0.5	/	/	/	/

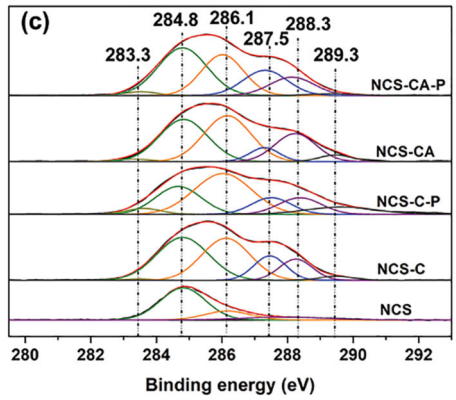

Figure 3.

(a) Full XPS spectra of different coatings and (b) elemental compositions detected on different coatings by XPS. Decrease in peak signal from Ca, Si, P, Ti, and O as well as increased signal of C and N indicates presence of collagen coating. (c) high-resolution spectra of C1s for different coatings further confirmed presence of collagen on nanorods.

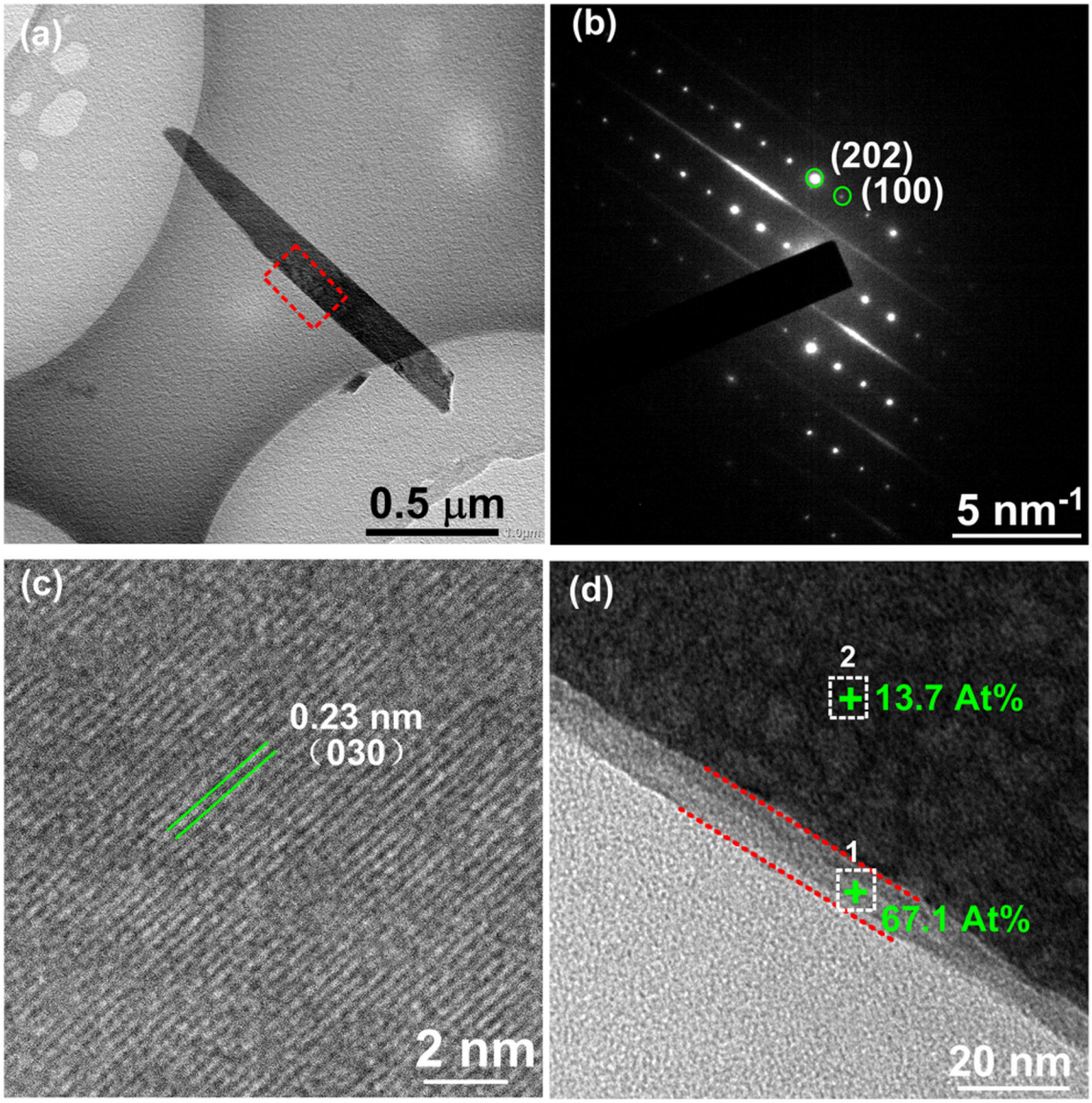

Figure 4.

TEM micrographs of the nanorods scratched from NCS-CA-P: (a) bright-field image (b) corresponding SAED pattern and. (c) HRTEM image of the nanorod confirm presence of 200–300 nm calcium sodium hydrogen silicate nanorods (d) enlarged image of the square marked in (a) of NCS-CA-P showing collagen shell and C content of the shell.

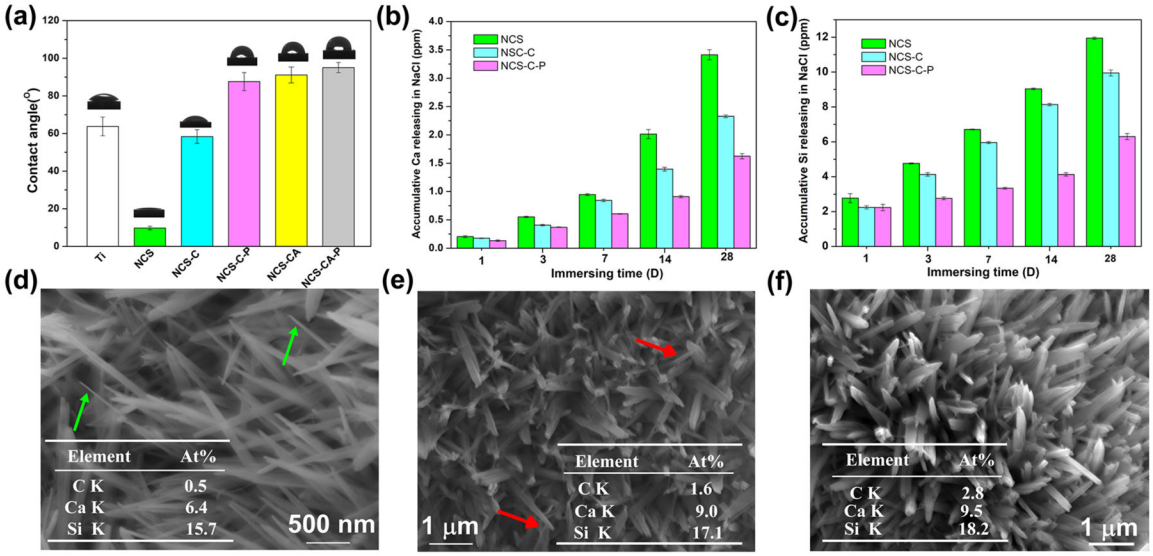

Figure 5.

(a) Contact angle and corresponding digital photograph of water droplets of different surfaces. PFHP-treated collagen shell increases hydrophobicity; (b) Ca and (c) Si release kinetics from NCS, NCS-C and NCS-C-P in 0.9 wt% NaCl for different immersion times show that PFHP-treated collagen shell (NCS-C-P) has the least amount of release. Surface morphologies of NCS (d), NCS-C (e) and NCS-C-P (f) after immersion in 0.9 wt% NaCl for 28 days; The tables inserted (d), (e) and (f) show the C, Ca, and Si amounts on the corresponding surfaces; arrows marked in (d) and (e) show the nanorods after significant degradation. PFHP treatment results in least degradation of nanorods.

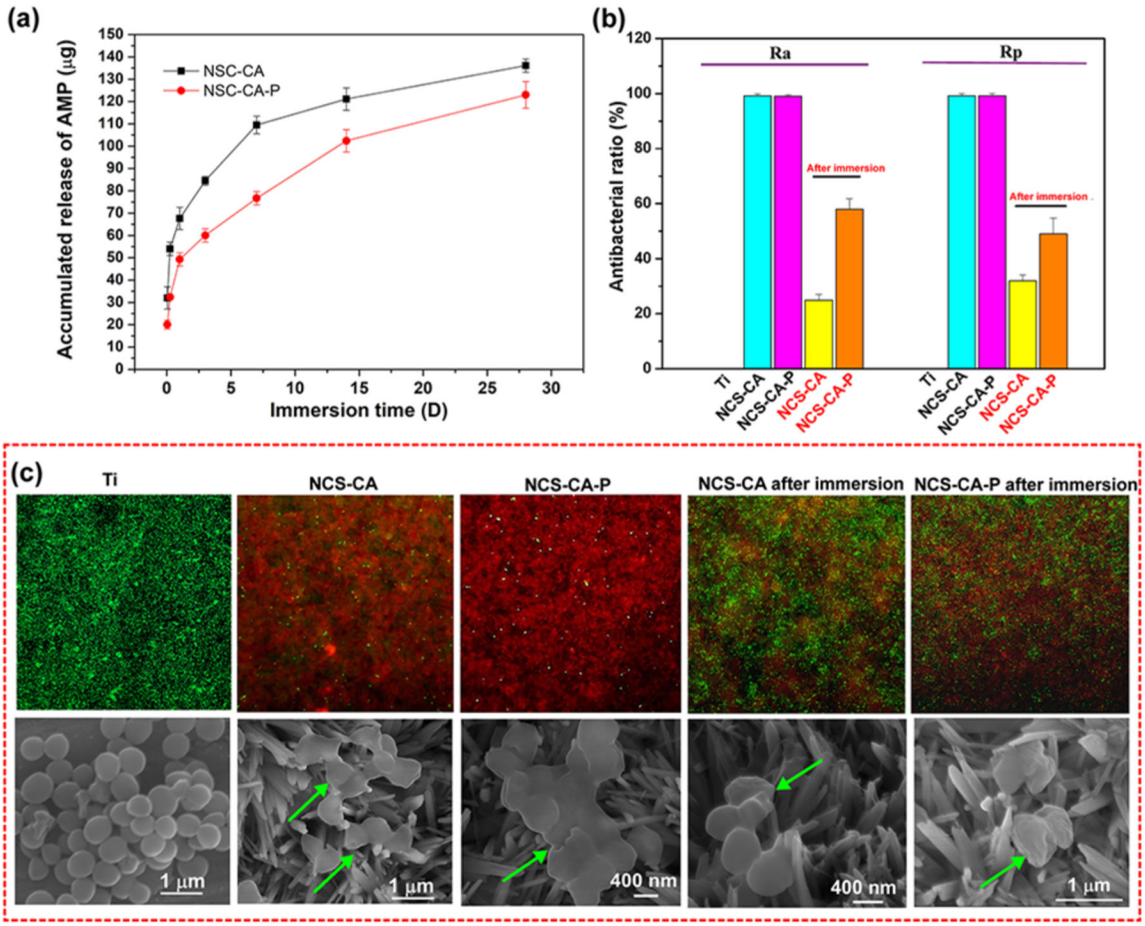

Figure 6.

(a) Cumulative release of AMP from NCS-CA and NCS-CA-P up to 28 days shows that PFHP treatment resulted in sustained release of AMP; (b) contact and release antibacterial ratio of NCS-CA and NCS-CA-P before and after immersion for 28 days shows that 60% toxicity towards adherent bacteria and 50% toxicity towards planktonic bacteria; (c) live-dead assay (upper row) and the corresponding SEM images (lower row) of S. aureus cultured on different surfaces after 24 h of incubation.

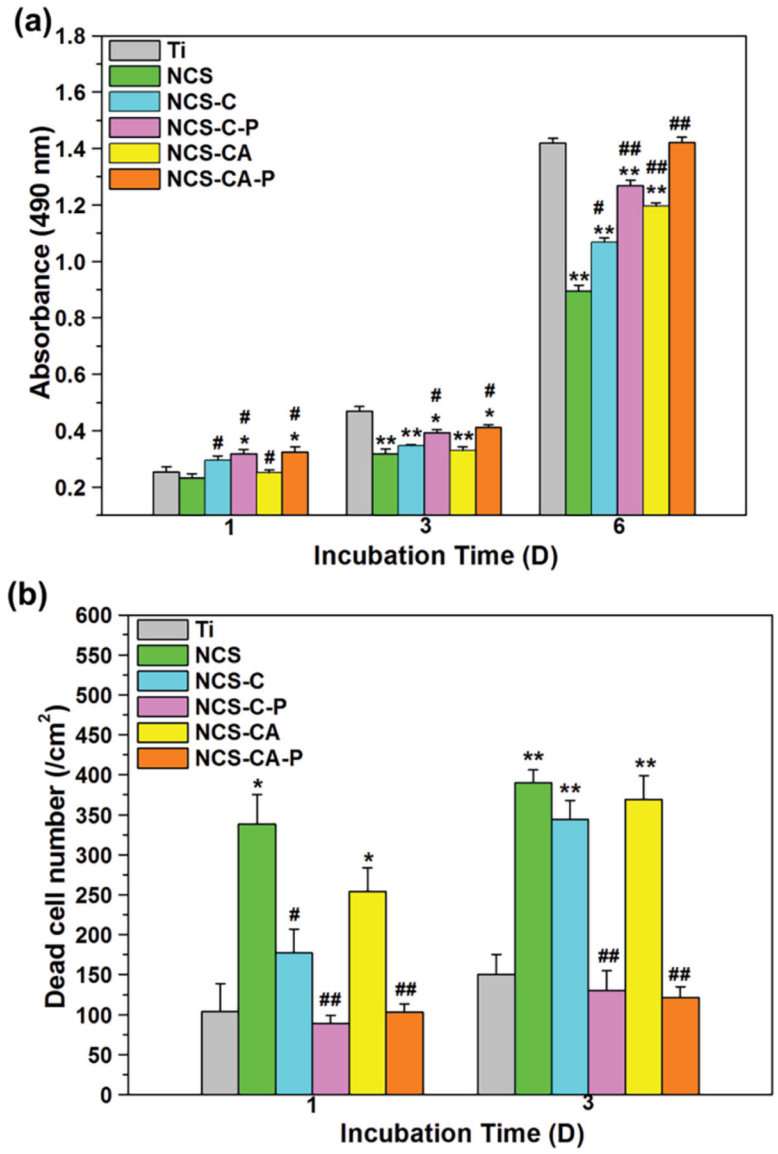

Figure 7.

(a)MTT assays of cell adhesion after 1 day and proliferation after 3 and 6 days of incubation on different surfaces; (b) dead cell numbers after 1 and 3 days of incubation on different surface. (*) $p<0.05$ and (**) $p<0.01$compared with Ti control, (#) $p < 0.05$ and (##) $p < 0.01$ compared with NCS. As can be seen, collagen shell enhances cytocompatibility. While AMP increases cytotoxicity, PFHP treatment mitigates this by regulating AMP release.

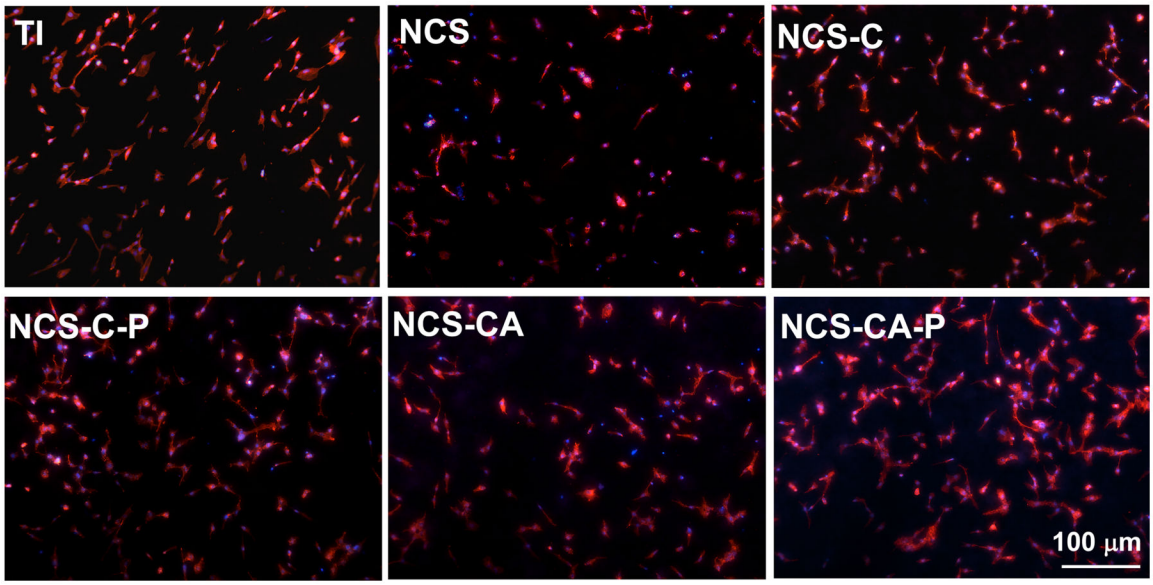

Figure 8.

Cell nucleus (blue) and actin (red) fluorescence images (merged channel) of osteoblasts after 24 h of culture on different surfaces. Cells show polygonal morphologies and organized actin bundles on collagen coated nanorods indicating enhanced cell adhesion.

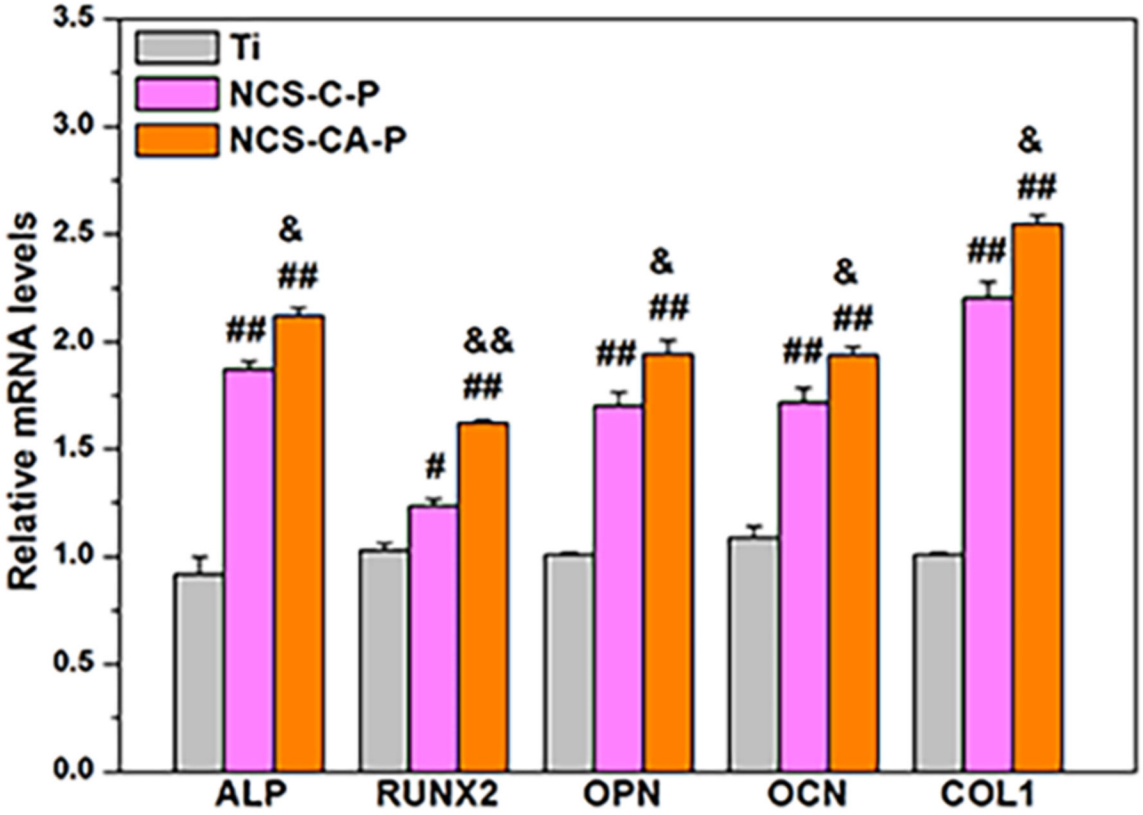

Figure 9.

Gene expressions of osteoblasts cultured on different surfaces after incubation for 14 days indicates accelerated cell differentiation on NCS-CA-P and NCS-C-P as compared to uncoated Ti. (#) $p<0.05$ and (##) $p<0.01$ compared with Ti, and (&) $p<0.05$ and (&&) $p<0.01$ compared with NCS-C-P.

Table 1.

Treatment process for fabricating different surfaces and labelling notations.

Sample Name	Spin-coating (I)		PFHP Treatment (II)
	Col-I (3 mg/mL)	AMP (6 mg/mL)	180 °C, 15 min
NCS-C	√		
NCS-C-P	√		√
NCS-CA	√	√	
NCS-CA-P	√	√	√